Electronic supplementary information

A-site cations in stannate perovskites affect their performance in catalysing CO_2 electroreduction

Guoqing Wang, Hao Yuan, Haiyan Zhang, Ruigang Liu, Shanhu Yue, Jiaxu Yan, Xiaoji Xie,* and Min Lu**

Chemicals

$MgCl_2 \cdot 6H_2O$, $BaCl_2 \cdot 2H_2O$, and $CaCl_2$ were obtained from Xilong Scientific Co., Ltd. $SrCl_2 \cdot 6H_2O$ and $Na_2SnO_3 \cdot 3H_2O$ were purchased from Shanghai Aladdin Bio-Chem Technology Co., Ltd. $NH_3 \cdot H_2O$ was obtained from Shanghai Lingfeng Chemical Reagent Co., Ltd. All gases were supplied by Nanjing Special Gas Factory Co., Ltd. Other chemicals were purchased from Nanjing WanQing Chemical Glassware Instrument Co., Ltd. Unless otherwise stated, all chemicals were used as received without further purification.

Catalyst preparation and characterizations

In order to obtain the desired $MSnO_3$ (M = Ba, Sr, and Ca) catalysts in high purity, four points need to be noted.[1,2] Firstly, the concentration of MCl_2 in the solution should not be too high. A high concentration of MCl_2 may result in $MSn(OH)_6$ as a multiphase precipitate. Secondly, the Na_2SnO_3 solution should be added in one batch. If the addition is carried out for a longer duration, ununiform morphologies emerge. Thirdly, the calcination temperature should be high enough. A low calcination temperature (e.g., 400 ºC) would result in amorphous $MSnO_3$. Finally, the calcination needs to be carried out in an Ar atmosphere. Calcination in the air would result in the by-product MCO_3.

The obtained $MSnO_3$ (M = Ba, Sr, and Ca) catalysts were characterized by powder X-ray diffraction (XRD), X-ray photoelectron spectroscopy (XPS), and energy-dispersive spectroscopy (EDS). No signals of other materials were observed, indicating the high purity of the obtained $MSnO_3$ catalysts.

Electroreduction of CO_2 and electrochemical characterizations

In a typical experiment, CO_2 reduction was carried out in an H-type gas-tight reactor with a Nafion 117 membrane using the electrolyte of $KHCO_3$ (0.1 mol L^{-1}, pH = 8.83) under continuous stirring at a rate of 500 rpm. A three-electrode mode was applied for the corresponding electrochemical characterizations, in which a Ag/AgCl, KCl (saturated) electrode, a platinum foil, and a catalyst-coated carbon plate were used as the reference electrode, the counter electrode, and the working electrode, respectively. The working electrode was fabricated through the direct coating of the catalyst as previously reported.[3] Specifically, a mixture of the catalyst, ethanol, and Nafion solution (5 mg catalyst, 150 μL ethanol, 20 μL 5% Nafion) was prepared and then modified onto

both sides of a carbon plate electrode by spin coating to achieve a loading of ~2 mg cm^{-2}. Prior to the CO_2R and corresponding electrochemical characterizations, a $KHCO_3$ solution (60 mL, 0.1 mol L^{-1}) was added into the reactor, leaving a headspace of 40 mL. The electrolyte was purged with N_2 for 30 min to remove air in the headspace. Subsequently, cyclic voltammetry (CV) was carried out from −0.6 to −2.0 V (vs. Ag/AgCl, KCl (saturated)) on an electrochemical workstation (CH Instruments, CHI 660 or Zahner, IM6) for 20 cycles at a scan rate of 50 mV s^{-1} to activate and stabilize the catalyst-electrolyte interface.

To obtain the faradaic efficiency (FE) and current density (j) of resulting products, a constant potential (−0.8, −0.9, −1.0, −1.1, −1.2, or −1.4 V vs. reversible hydrogen electrode (RHE)) was applied at the working electrode for 1800 s. After the electrolysis, both gaseous and liquid products were collected for quantification. Gaseous products were analyzed by a gas chromatograph (Shimadzu, GC-2014), and liquid products were analyzed by a liquid chromatograph (Hitachi, Primaide). The FE, indicating the product selectivity, was calculated according to the following equation.

$$FE = (n \times z \times F)/Q \quad \text{(S1)}$$

where n is the molar amount of a product (in the unit of mol), z is the number of electrons consumed to produce one product molecule (z = 2 for the product of CO, HCOOH, and H_2), F is the Faraday constant (F = 96500 C mol^{-1}), and Q is the number of electrons consumed during electrolysis (in the unit of C).

The long-term stability of the catalysts was checked under similar conditions. After the activation and stabilization of the catalyst-electrolyte interface by CV, a constant potential, −1.2 V (vs. RHE), was applied at the working electrode for 10 h under CO_2 bubbling. The electrolysis was paused every 3600 s, and liquid products were collected and analyzed by a liquid chromatograph. Besides, to study the stability of the catalysts, the working electrodes were collected, gently rinsed with water, and characterized before any test, after CV activation, after electrolyzing at the potential of −0.8, −0.9, −1.0, −1.1, −1.2, and −1.4 V for 1800 s each (the study of selectivity and activity), and after the long-term stability test.

Notably, all potentials reported in this study were referred to the RHE unless otherwise noted. Potentials applied versus the Ag/AgCl electrode ($E_{Ag/AgCl}$) were converted into potentials versus the RHE (E_{RHE}) by the following equation.

$$E_{RHE} = E_{Ag/AgCl} + 0.197 + 0.059 \times pH \quad (S2)$$

Computational methods

All the first-principle calculations were carried out based on the density functional theory (DFT), using the Vienna ab initio simulation package (VASP) code.[4–6] The ion-electron interactions were described by the projector augmented wave method, and the generalized gradient approximation in the Perdew-Burke-Ernzerhof form and the cut-off energy of 500 eV for the plane-wave basis set were adopted.[7] Free energies of reaction intermediates were calculated on the surface of thermodynamically stable (001) perovskite.[8] A vacuum layer of ~10 Å was employed above the surface to avoid the interaction between two periodic units. The atomic positions in the outermost five atomic layers were fully relaxed at least, while the remaining atoms were kept fixed to their bulk-like structures. During the structure relaxation, the convergence threshold was 10^{-4} eV and 1×10^{-3} eV $Å^{-1}$ for energy and force, respectively. The Monkhorst-Pack K-point mesh was set as 2 × 2 × 1 for reaction intermediates and 4 × 4 × 4 for structure relaxation of perovskite oxides. The free energy (G) of each reaction intermediate can be calculated by the following equation.

$$G = E_{DFT} + \int C_p dT + ZPE - TS \quad (S3)$$

where E_{DFT} is the free energy obtained directly from calculations, $\int C_p dT$ is the enthalpy, ZPE is zero-point energy, T is the temperature of 298.15 K, and S is the entropy. Using the VASPKIT program, post-calculation was carried out to derive the free energy correction term ($\int C_p dT$ + ZPE − TS) and to obtain the free energy. The free energy change (ΔG) for each elementary reaction was on the basis of the computational hydrogen electrode model,[9] and calculated by $\Delta G = G_{product} - G_{reactant}$.

The limiting potential (U_L) was calculated by the following equation.

$$U_L = -\Delta G_{max}/e \quad (S4)$$

where ΔG_{max} is the maximum free energy change in all steps of the energy pathway.

Our electrochemical stability calculations (Pourbaix diagrams) were performed using the Materials Project database according to the workflow detailed in a previous report.[10]

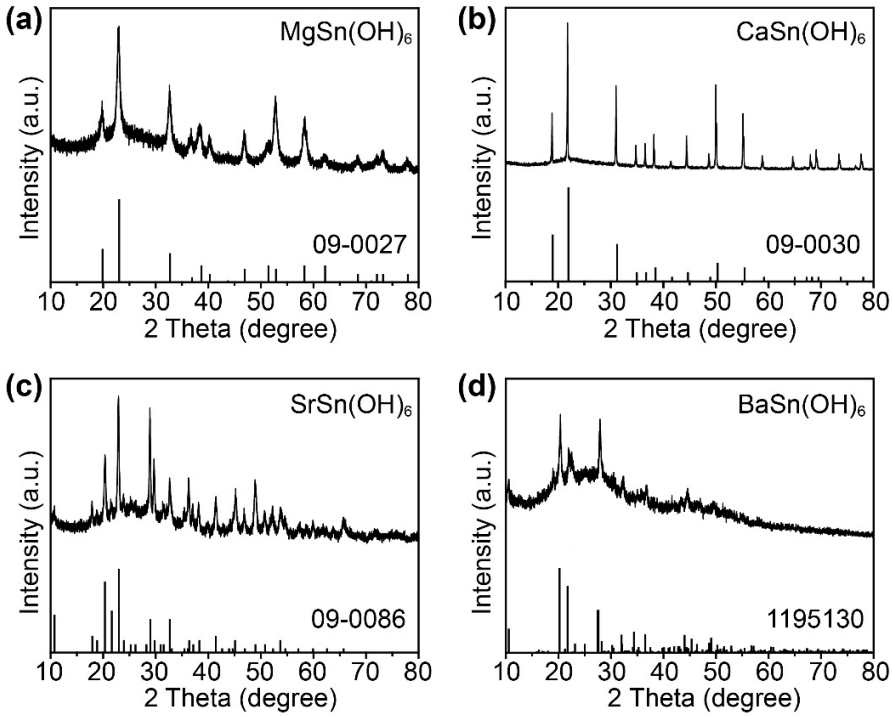

Figure S1. XRD patterns of $MSn(OH)_6$ (M = Mg, Ca, Sr, and Ba) precursors. (a) $MgSn(OH)_6$, (b) $CaSn(OH)_6$, (c) $SrSn(OH)_6$, and (d) $BaSn(OH)_6$. The pattern at the bottom of each panel is the corresponding literature reference ($MgSn(OH)_6$: JCPDS 09-0027, $CaSn(OH)_6$: JCPDS 09-0030, $SrSn(OH)_6$: JCPDS 09-0086, and $BaSn(OH)_6$: MP 1195130).

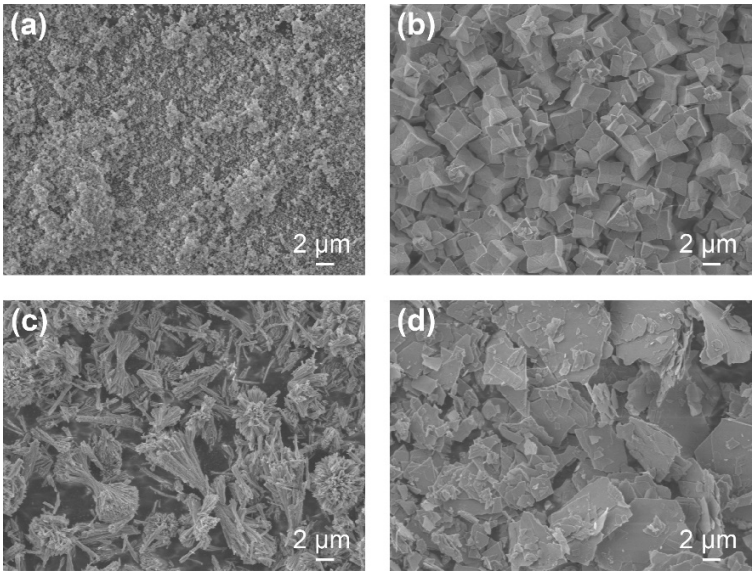

Figure S2. SEM images of $MSn(OH)_6$ (M = Mg, Ca, Sr, and Ba) precursors. (a) $MgSn(OH)_6$, (b) $CaSn(OH)_6$, (c) $SrSn(OH)_6$, and (d) $BaSn(OH)_6$.

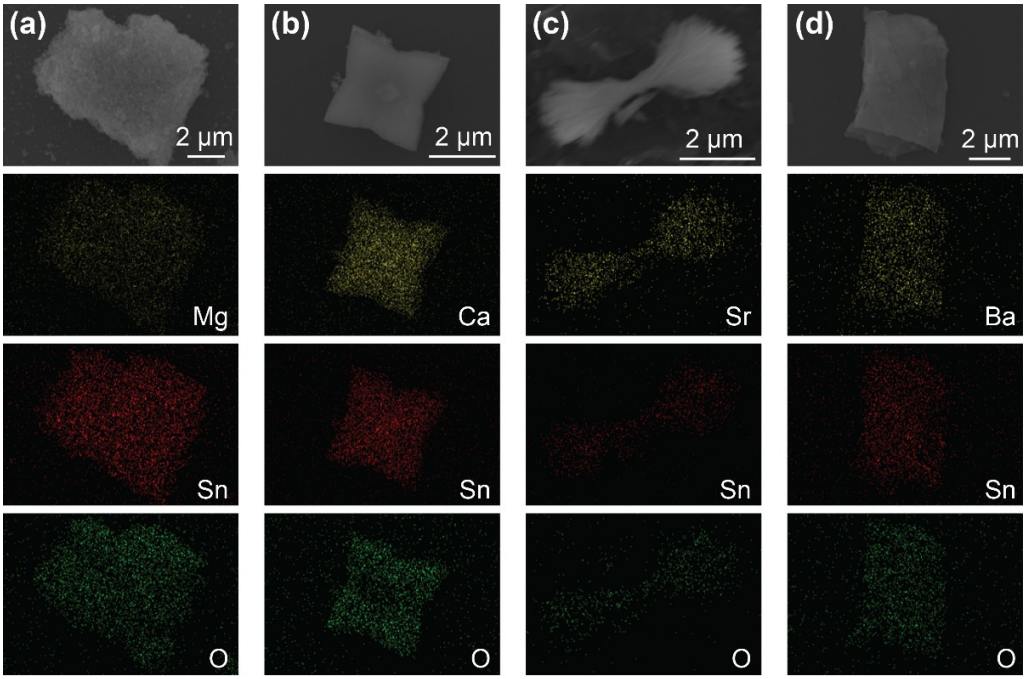

Figure S3. Elemental mapping of $MSnO_3$-700 (M = Mg, Ca, Sr, and Ba) catalysts by energy-dispersive spectroscopy. (a) $MgSnO_3$-700, (b) $CaSnO_3$-700, (c) $SrSnO_3$-700, and (d) $BaSnO_3$-700.

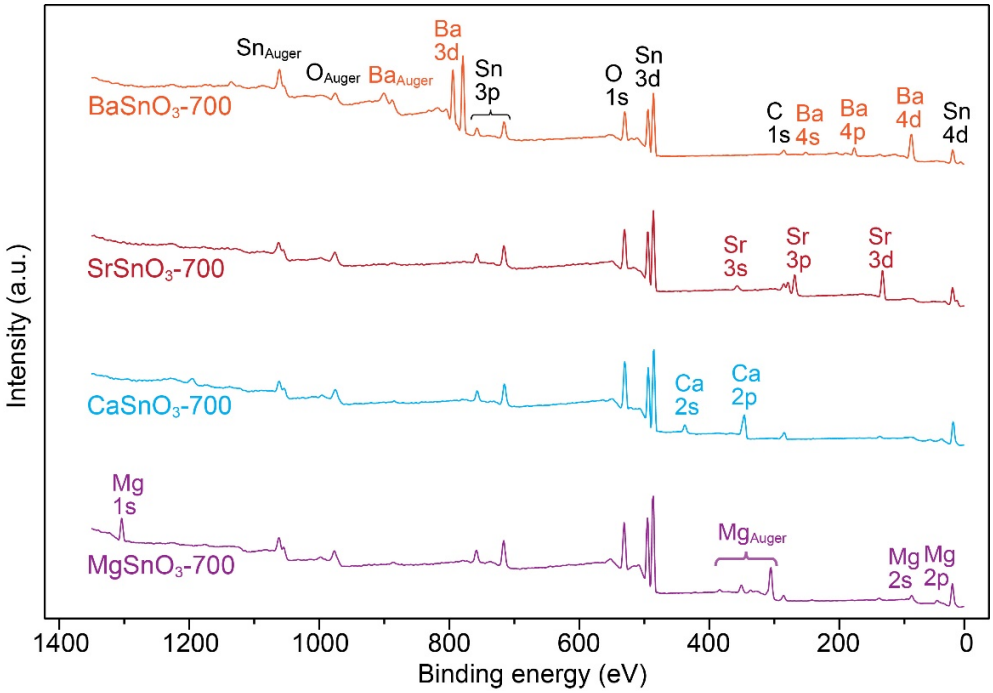

Figure S4. XPS survey spectra of $MSnO_3$-700 (M = Mg, Ca, Sr, and Ba) catalysts.

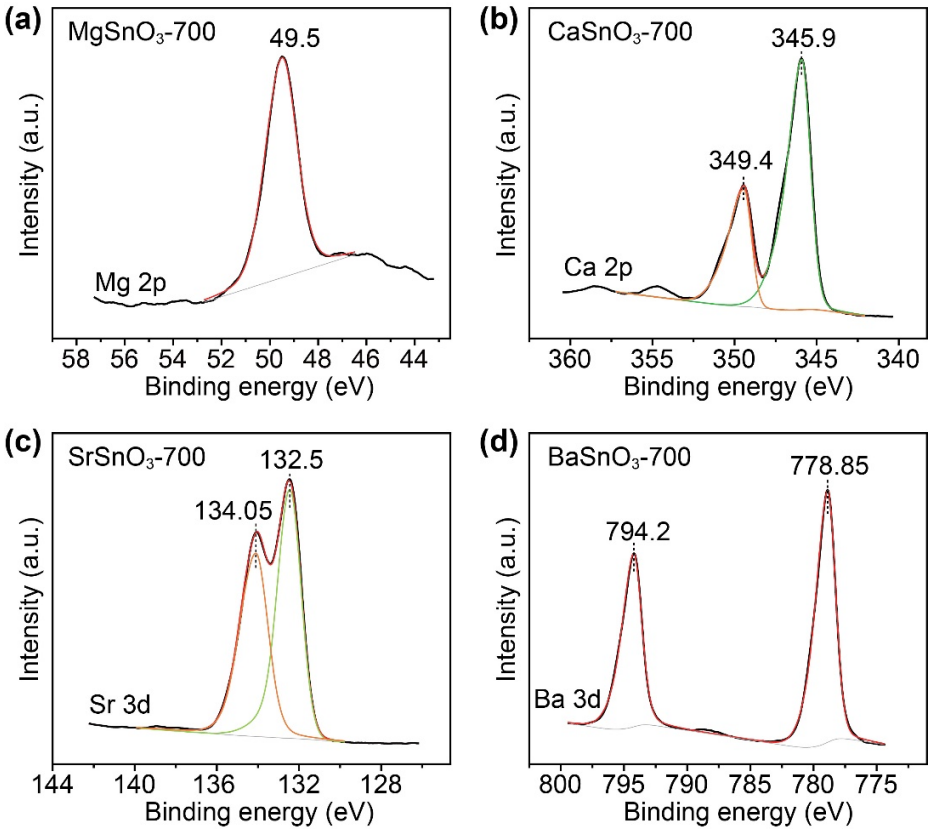

Figure S5. High-resolution XPS spectra (black lines) of the M element in $MSnO_3$-700 (M = Mg, Ca, Sr, and Ba) catalysts. (a) $MgSnO_3$-700, (b) $CaSnO_3$-700, (c) $SrSnO_3$-700, and (d) $BaSnO_3$-700. Colored lines are the deconvolution results.

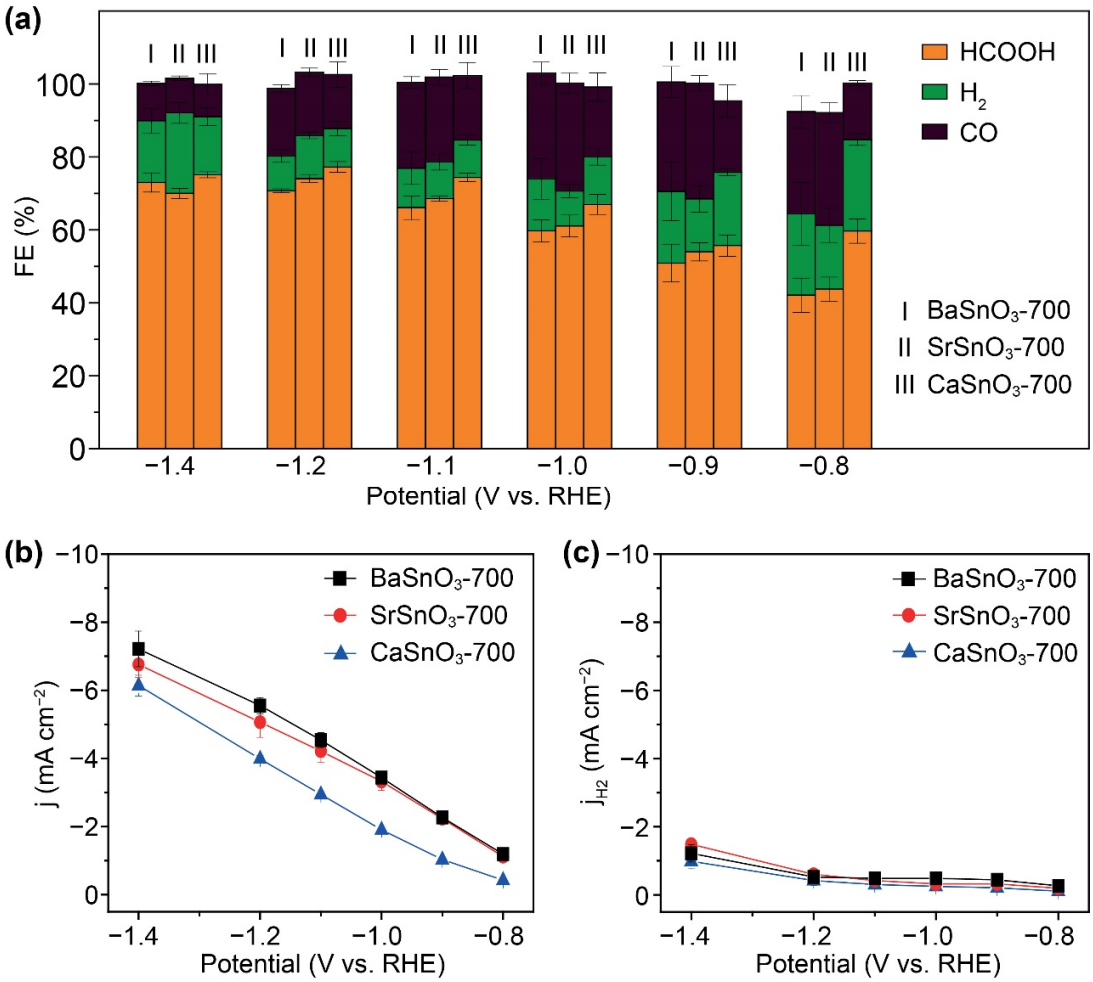

Figure S6. (a) FEs toward HCOOH, H_2, and CO over $MSnO_3$-700 (M = Ca, Sr, and Ba) catalysts during bulk electrolysis. (b, c) Corresponding (b) total current density and (c) partial current density of H_2 over $MSnO_3$-700 catalysts.

Table S1. Catalytic performance of $MSnO_3$-700 (M = Ba, Sr, and Ca) catalysts and similar catalytsts reported previously.[a]

Catalyst	Electrolyte	Potential (V vs. RHE)	FE_{HCOOH} (%)	j_{HCOOH} (mA cm^{-2})[b]	Stability	Ref.
$BaSnO_3$-700	0.1 M $KHCO_3$	−1.2	70.7	3.93	Poor (10 h test)[c]	This work
$SrSnO_3$-700	0.1 M $KHCO_3$	−1.2	74.0	3.75	Media (10 h test)[c]	This work
$CaSnO_3$-700	0.1 M $KHCO_3$	−1.2	77.3	3.08	Good (10 h test)[c]	This work
$SrSnO_3$ nanowires	0.5 M $NaHCO_3$	−1.3	80.1	21.6	Good (10 h test) may partially degrade[d]	[11]
Bulk $SrSnO_3$	0.5 M $NaHCO_3$	−1.0	73.8	11	–	[11]
$Ba_{0.5}Sr_{0.5}SnO_3$	1 M KOH	−1.2	90.9	169.1	Remarkable (15 h test) may partially degrade[d]	[12]

[a] Generally, the catalytic performance of $MSnO_3$-700 (M = Ba, Sr, and Ca) catalysts is comparable to that of previously reported Sn-based catalysts.[13] Notably, it is difficult to make direct comparisons of the catalytic performance, particularly the catalytic activity and stability of catalysts, as different studies are usually carried out under different conditions (e.g., reactor design). The reaction conditions can affect the catalyst's performance.

[b] The partial current density of HCOOH is related to many factors, such as reactor design.

[c] The stability of the catalyst is the relative stability compared with the stabilities of the other two $MSnO_3$-700 catalysts.

[d] The stability is adopted directly from the reference. The annotation "may partially degrade" is deduced according to the results provided in the reference.

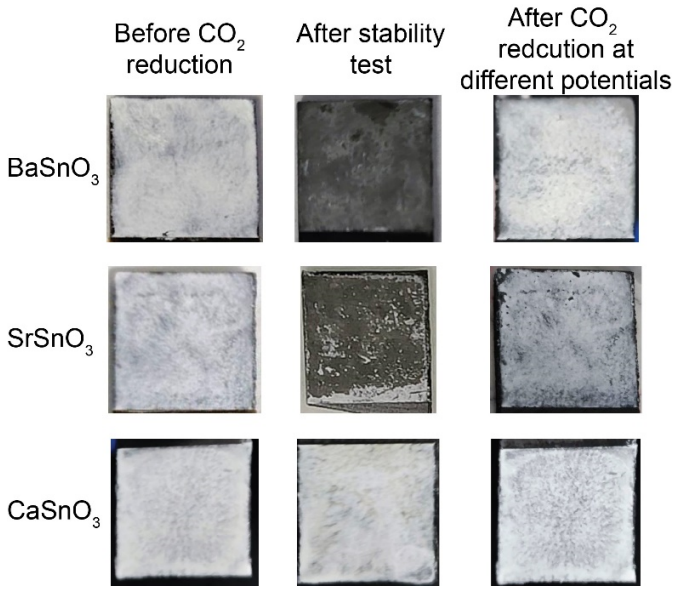

Figure S7. Typical photos of carbon plates loaded with $MSnO_3$-700 (M = Ba, Sr, and Ca) catalysts (working electrodes) before and after CO_2 reduction under different conditions. Photos in the middle panel were taken after continuous CO_2 reduction for 10 h (the stability test). Photos in the right panel were taken after the study of selectivity and activity (working electrodes worked at potentials of −0.8, −0.9, −1.0, −1.1, −1.2, and −1.4 V for 1800 s each).

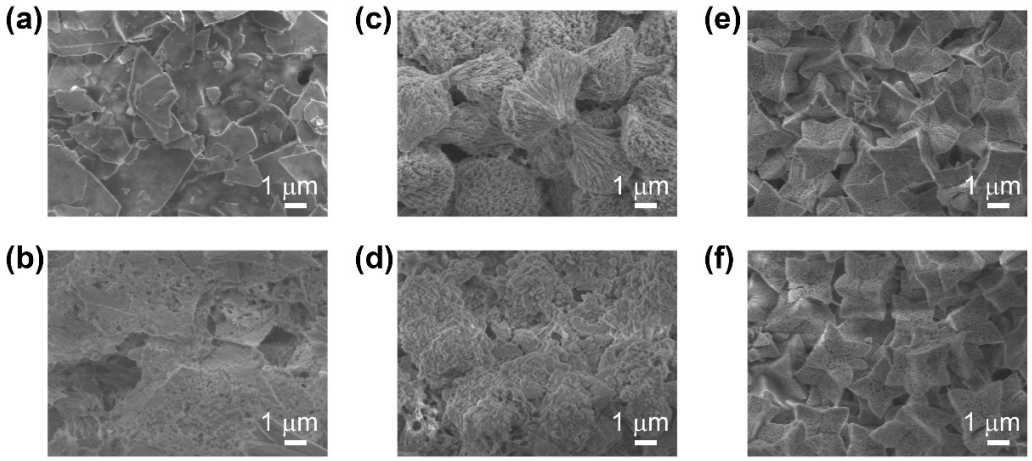

Figure S8. Typical SEM images of the $MSnO_3$-700 (M = Ba, Sr, and Ca) catalyst-coated working electrodes (a, c, e) before and (b, d, f) after the long-term stability test. (a, b) $BaSnO_3$-700, (c, d) $SrSnO_3$-700, and (e, f) $CaSnO_3$-700.

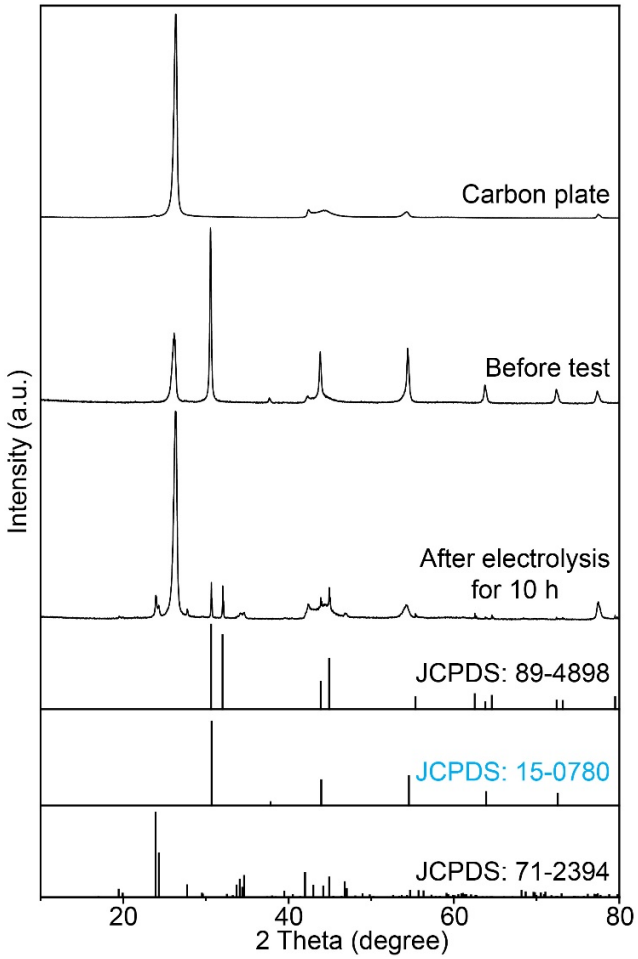

Figure S9. XRD patterns of bare carbon plate, $BaSnO_3$-700 loaded carbon plate (working electrode) before any test, and $BaSnO_3$-700 loaded carbon plate after continuous CO_2 reduction for 10 h (the stability test). Patterns at the bottom are literature references for Sn (JCPDS 89-4898), $BaSnO_3$ (JCPDS 15-0780), and $BaCO_3$ (JCPDS 71-2394).

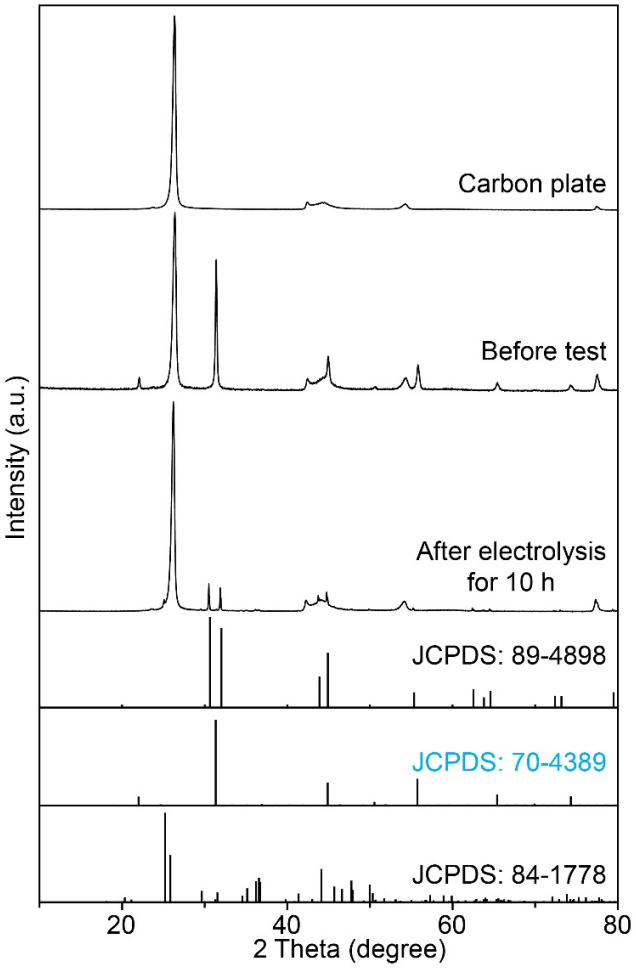

Figure S10. XRD patterns of bare carbon plate, $SrSnO_3$-700 loaded carbon plate (working electrode) before any test, and $SrSnO_3$-700 loaded carbon plate after continuous CO_2 reduction for 10 h (the stability test). Patterns at the bottom are literature references for Sn (JCPDS 89-4898), $SrSnO_3$ (JCPDS 70-4389), and $SrCO_3$ (JCPDS 84-1778). The pattern of bare carbon plate is the same as that shown in Figure S9 and used as a reference here.

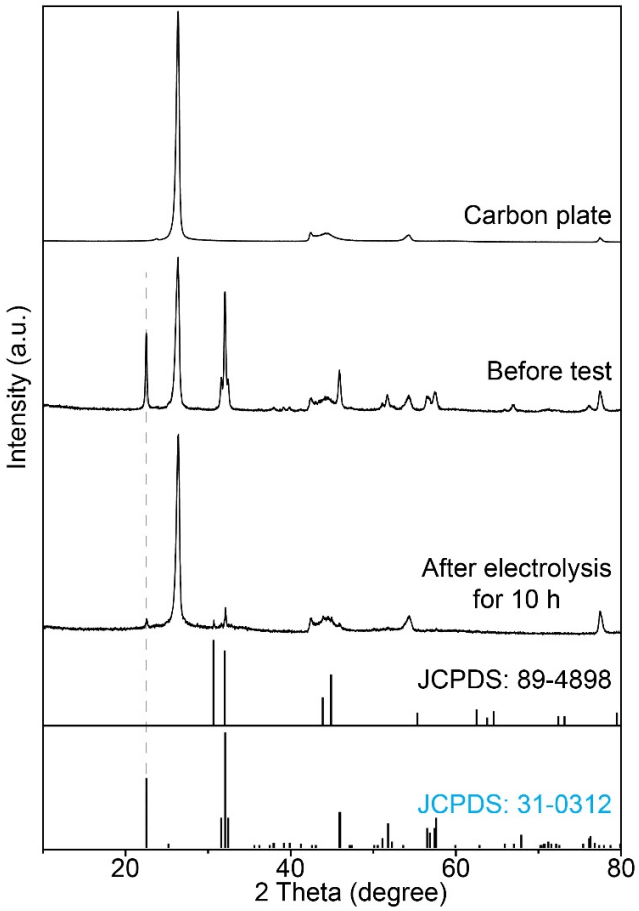

Figure S11. XRD patterns of bare carbon plate, $CaSnO_3$-700 loaded carbon plate (working electrode) before any test, and $CaSnO_3$-700 loaded carbon plate after continuous CO_2 reduction for 10 h (the stability test). Patterns at the bottom are literature references for Sn (JCPDS 89-4898) and $CaSnO_3$ (JCPDS 31-0312). The dashed line indicates the presence of $CaSnO_3$-700. The pattern of bare carbon plate is the same as that shown in Figure S9 and used as a reference here.

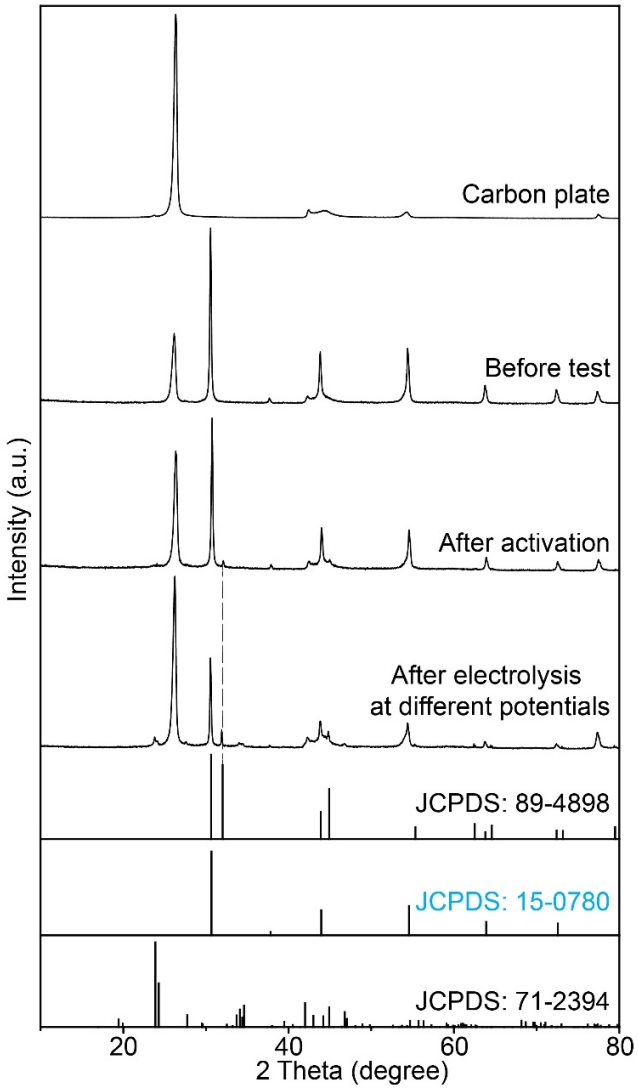

Figure S12. XRD patterns of bare carbon plate, $BaSnO_3$-700 loaded carbon plate (working electrode) before any test, $BaSnO_3$-700 loaded carbon plate after CV activation, and $BaSnO_3$-700 loaded carbon plate after electrolyzing at the potential of −0.8, −0.9, −1.0, −1.1, −1.2, and −1.4 V for 1800 s each (the study of selectivity and activity). Patterns at the bottom are literature references for Sn (JCPDS 89-4898), $BaSnO_3$ (JCPDS 15-0780), and $BaCO_3$ (JCPDS 71-2394). The dashed line indicates the presence of Sn. Notably, on the basis of the XRD results, it is difficult to determine the presence of $BaSnO_3$-700 after the study of selectivity and activity because some peaks of $BaSnO_3$ almost overlap with those of Sn. According to the intensity ratio of the two peaks at ~30.5 and 32 degrees, we may deduce that some $BaSnO_3$-700 remained on the working electrode after the study of selectivity and activity. The patterns of bare carbon plate and working electrode before any test are the same as those shown in Figure S9 and used as references here.

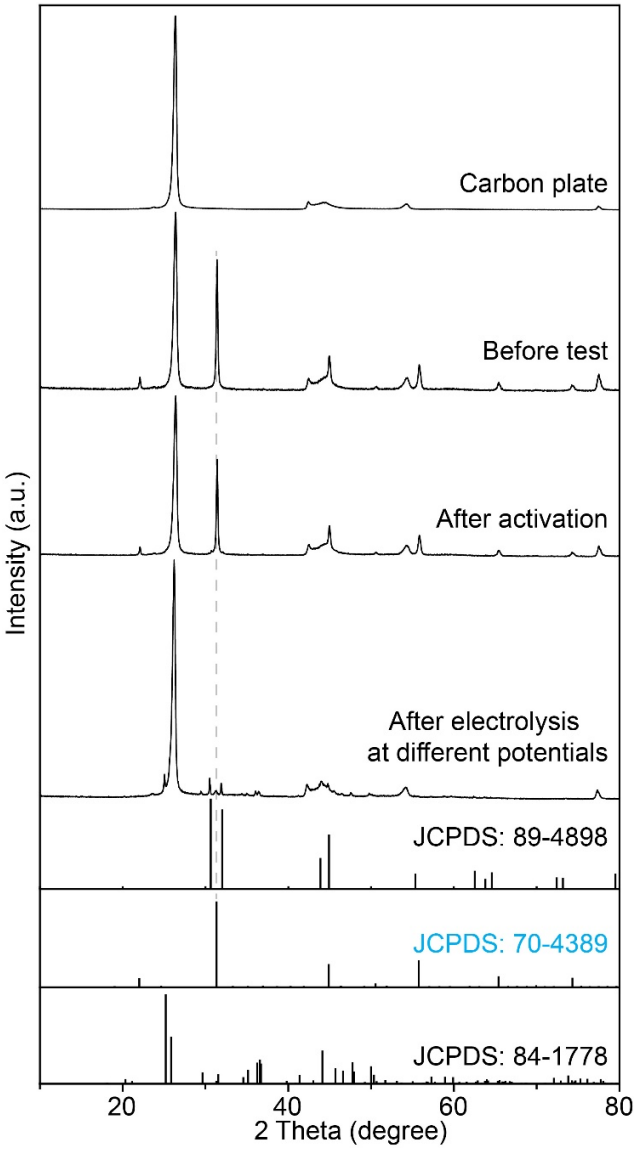

Figure S13. XRD patterns of bare carbon plate, $SrSnO_3$-700 loaded carbon plate (working electrode) before any test, $SrSnO_3$-700 loaded carbon plate after CV activation, and $SrSnO_3$-700 loaded carbon plate after electrolyzing at the potential of −0.8, −0.9, −1.0, −1.1, −1.2, and −1.4 V for 1800 s each (the study of selectivity and activity). Patterns at the bottom are literature references for Sn (JCPDS 89-4898), $SrSnO_3$ (JCPDS 70-4389), and $SrCO_3$ (JCPDS 84-1778). The dashed line indicates the presence of $SrSnO_3$-700. The patterns of bare carbon plate and working electrode before any test are the same as those shown in Figure S10 and used as references here.

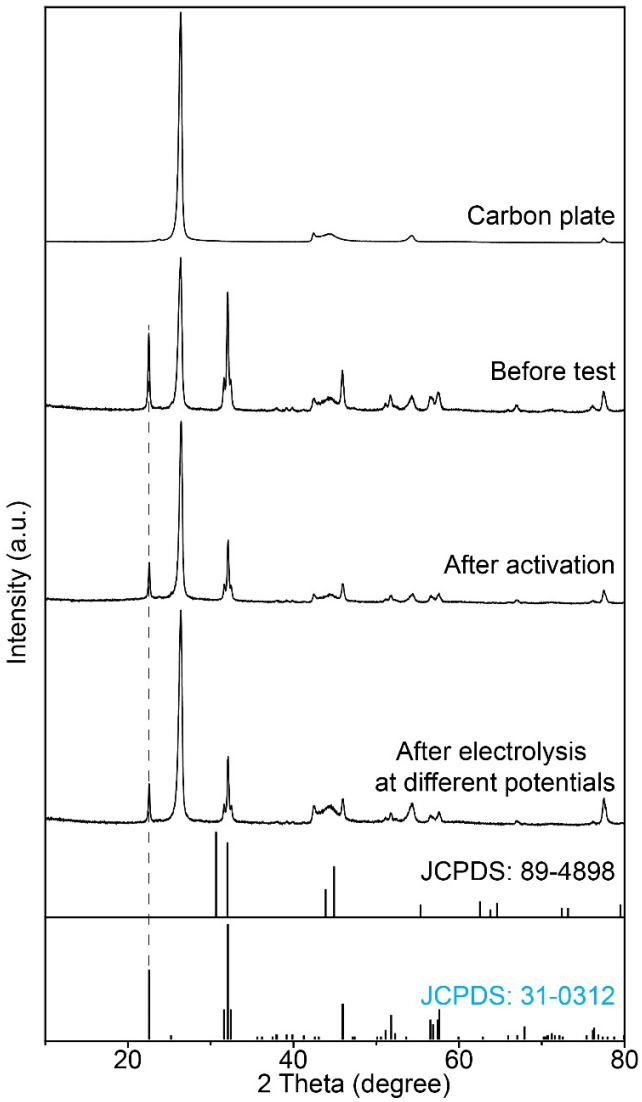

Figure S14. XRD patterns of bare carbon plate, $CaSnO_3$-700 loaded carbon plate (working electrode) before any test, $CaSnO_3$-700 loaded carbon plate after CV activation, and $CaSnO_3$-700 loaded carbon plate after electrolyzing at the potential of −0.8, −0.9, −1.0, −1.1, −1.2, and −1.4 V for 1800 s each (the study of selectivity and activity). Patterns at the bottom are literature references for Sn (JCPDS 89-4898) and $CaSnO_3$ (JCPDS 31-0312). The dashed line indicates the presence of $CaSnO_3$-700. The patterns of bare carbon plate and working electrode before any test are the same as those shown in Figure S11 and used as references here.

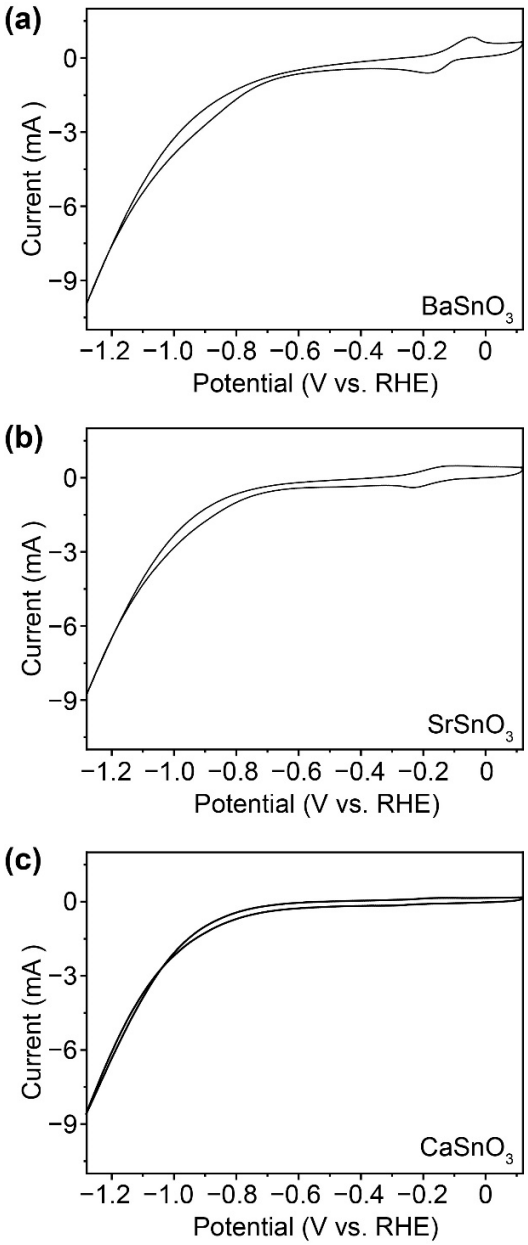

Figure S15. Typical cyclic voltammograms during the activation (5th cycle) of (a) $BaSnO_3$-700, (b) $SrSnO_3$-700, and (c) $CaSnO_3$-700 catalysts, respectively.

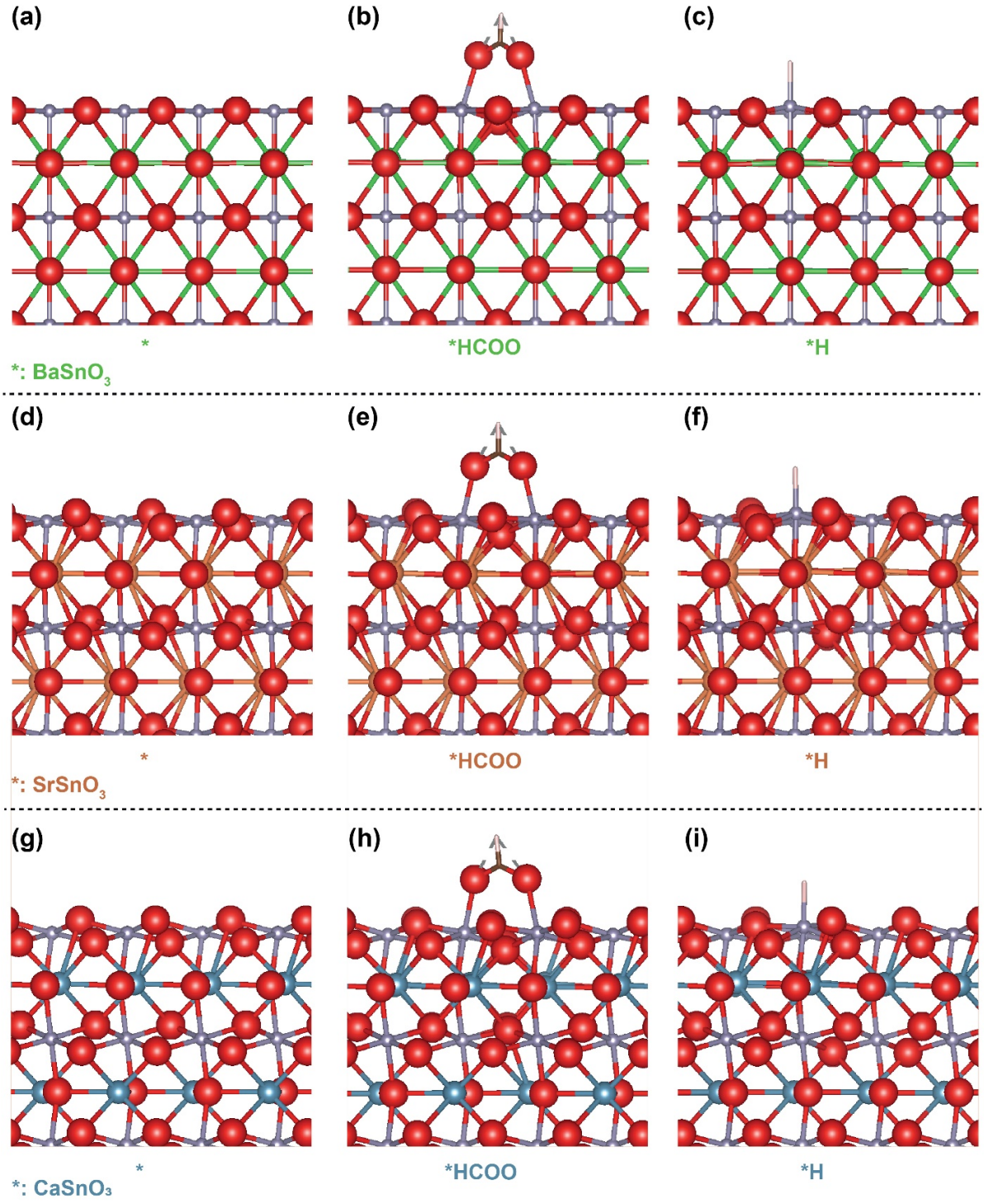

Figure S16. (a, d, g) Stable configurations of $MSnO_3$ slabs (*), (b, e, h) corresponding CO_2R reaction intermediates (*HCOO), and (c, f, i) corresponding HER intermediates (*H) determined by density functional theory.

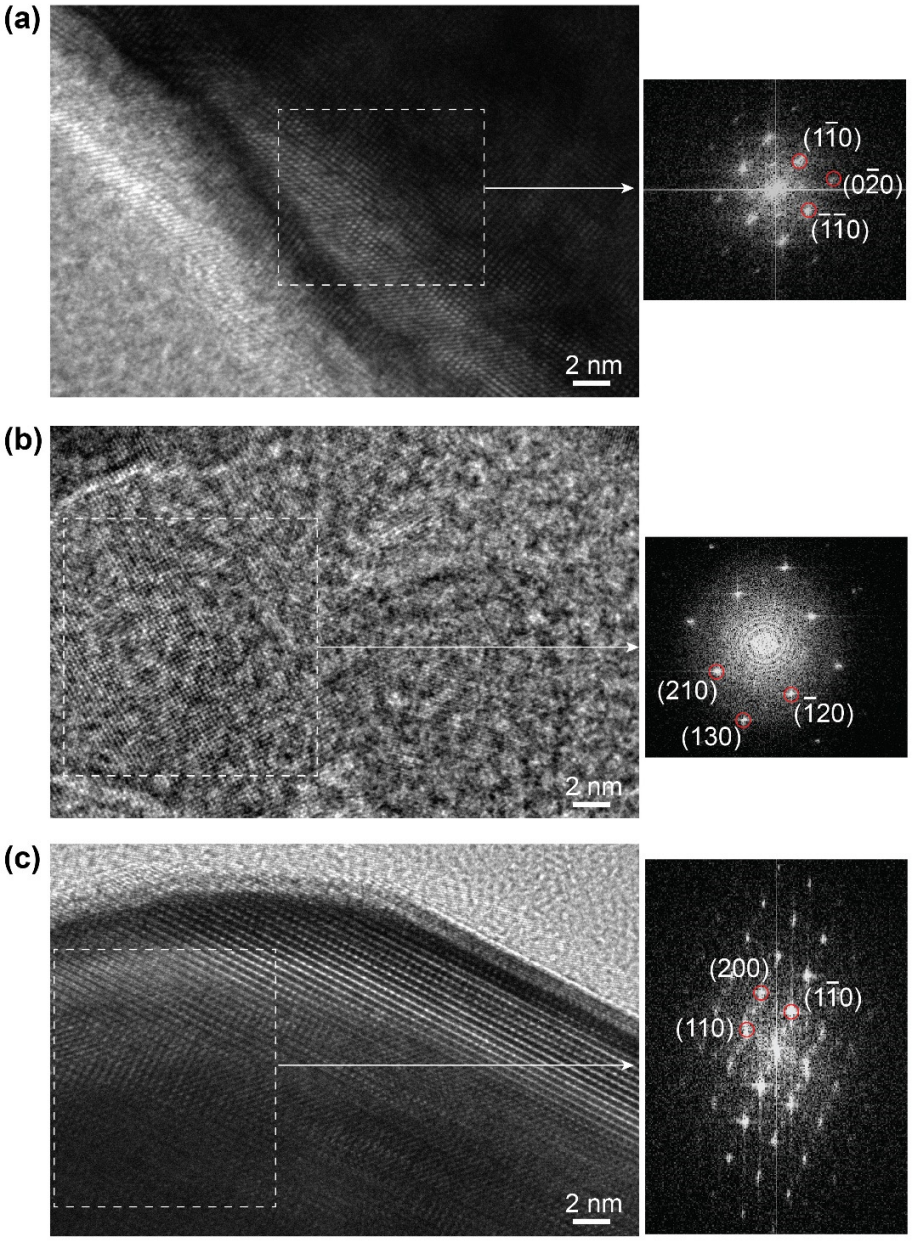

Figure S17. HRTEM images of a randomly selected part of (a) $BaSnO_3$-700, (b) $SrSnO_3$-700 and (c) $CaSnO_3$-700 catalysts and the corresponding fast Fourier transform (FFT) images of the dashed box in the HRTEM images. Due to the large size of these catalysts, the HRTEM images of the $BaSnO_3$-700 and $CaSnO_3$-700 catalysts were taken near the edge of the selected samples. The $SrSnO_3$-700 catalyst was sonicated and then loaded onto a TEM grid for HRTEM analysis. In addition, we tried to select flat samples/surfaces for the analysis. FFT images of these HRTEM images show that the zone axis can be (001).[14] Thus, the (001) plane of these catalysts can be an exposed plane.

Table S2. Calculated limiting potentials of CO_2R reaction and HER.

	$U_{L(CO2RR)}$ (V)	$U_{L(HER)}$ (V)
$BaSnO_3$	−0.92	−1.14
$SrSnO_3$	−0.99	−1.47
$CaSnO_3$	−1.07	−1.66

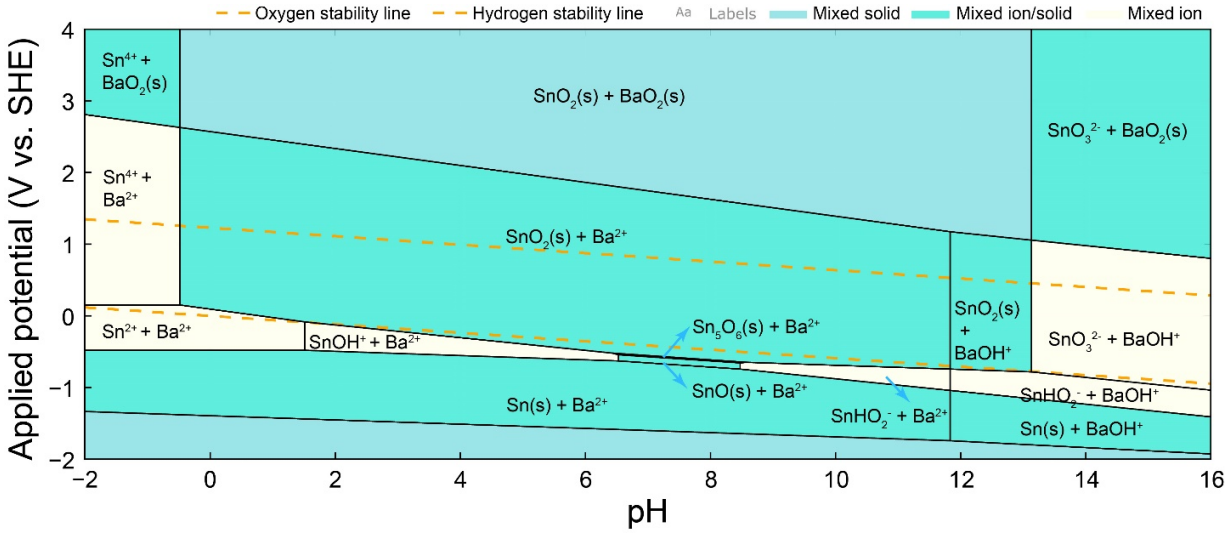

Figure S18. Calculated Pourbaix diagram of the Ba−Sn−O system.[10,15] The mixed solid at the bottom of the diagram is Sn(s) + BaH_2(s).

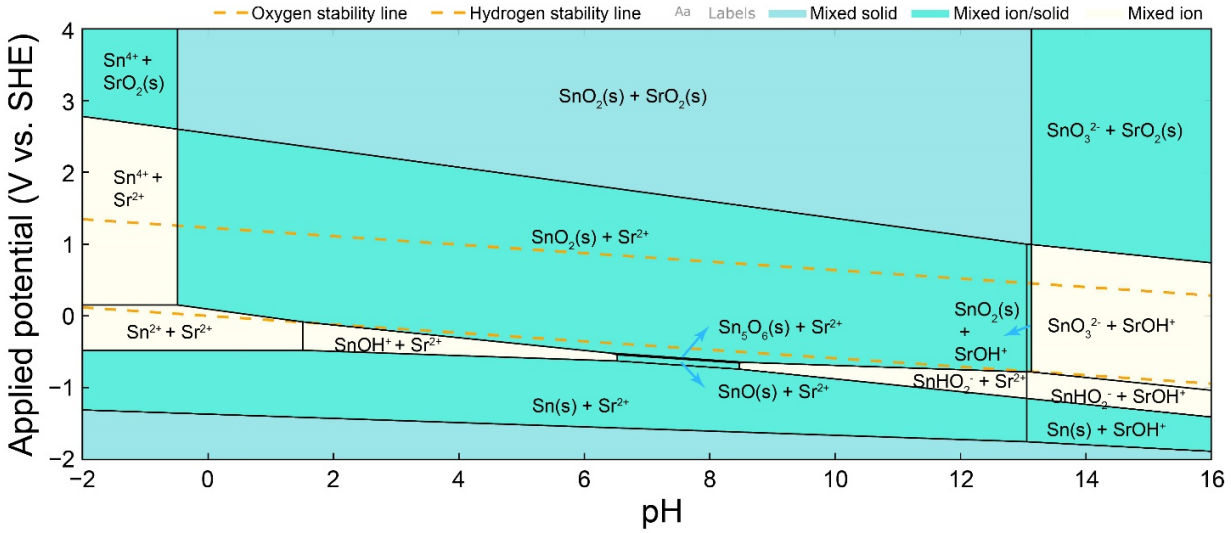

Figure S19. Calculated Pourbaix diagram of the Sr−Sn−O system.[10,15] The mixed solid at the bottom of the diagram is Sn(s) + SrH_2(s).

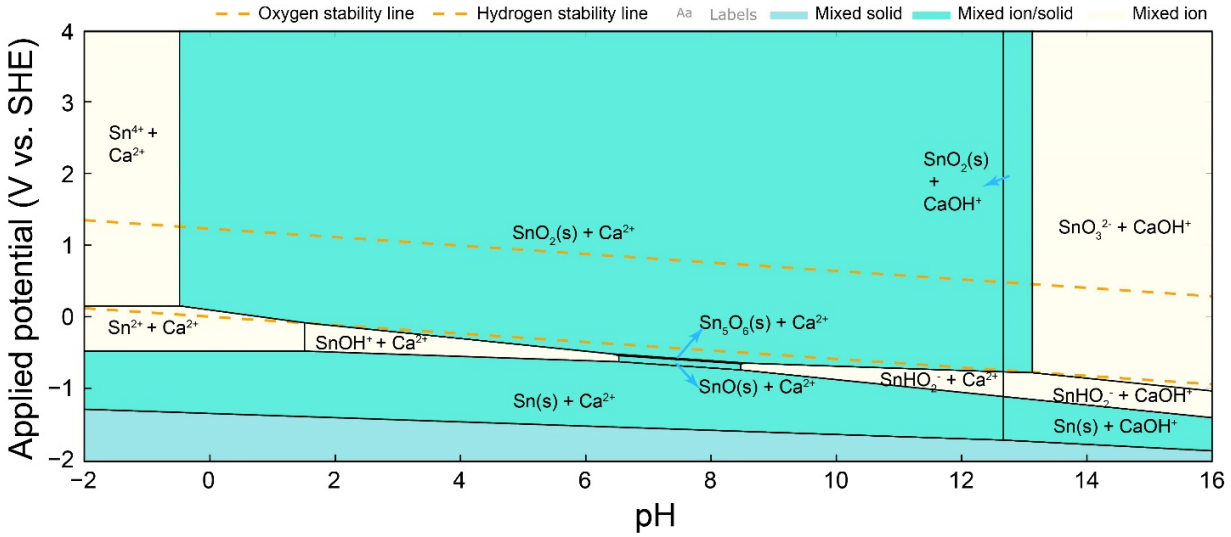

Figure S20. Calculated Pourbaix diagram of the Ca−Sn−O system.[10,15] The mixed solid at the bottom of the diagram is Sn(s) + CaH_2(s).

References:

[1] S.-L. Zhong, R. Xu, L. Wang, Y. Li, L.-F. Zhang, *Mater. Res. Bull.* **2011**, *46*, 2385.

[2] M. Inagaki, T. Kuroishi, Y. Yamashita, M . Urata, Z. *Anorg. Allg. Chem.* **1985**, *527*, 193.

[3] M. Chen, S. Wang, H. Zhang, P. Zhang, Z. Tian, M. Lu, X. Xie, L. Huang, W. Huang, *Nano Res.* **2020**, *13*, 729.

[4] G. Kresse, J. Hafner, *Phys. Rev. B* **1993**, *47*, 558.

[5] G. Kresse, J. Furthmüller, *Comp. Mater. Sci.* **1996**, *6*, 15.

[6] G. Kresse, J. Furthmüller, *Phys. Rev. B* **1996**, *54*, 11169.

[7] J. P. Perdew, J. A. Chevary, S. H. Vosko, K. A. Jackson, M. R. Pederson, D. J. Singh, C. Fiolhais, *Phys. Rev. B* **1992**, *46*, 6671.

[8] J. Hwang, K. Akkiraju, J. Corchado-García, Y. Shao-Horn, *J. Phys. Chem. C* **2019**, *123*, 24469.

[9] A. A. Peterson, F. Abild-Pedersen, F. Studt, J. Rossmeisl, J. K. Nørskov, *Energy Environ. Sci.* **2010**, *3*, 1311.

[10] A. K. Singh, L. Zhou, A. Shinde, S. K. Suram, J. H. Montoya, D. Winston, J. M. Gregoire, K. A. Persson, *Chem. Mater.* **2017**, *29*, 10159.

[11] Y. Pi, J. Guo, Q. Shao, X. Huang, *Nano Energy* **2019**, *62*, 861.

[12] M. Chen, K. Chang, Y. Zhang, Z. Zhang, Y. Dong, X. Qiu, H. Jiang, Y. Zhu, J. Zhu, *Angew. Chem. Int. Ed.* **2023**, *62*, e202305530.

[13] Y. Yao, W. Zhuang, R. Li, K. Dong, Y. Luo, X. He, S. Sun, S. Alfaifi, X. Sun, W. Hu, *Chem. Commun.* **2023**, *59*, 9017.

[14] M. Klinger, *J. Appl. Crystallogr.* **2017**, *50*, 1226.

[15] A. Jain, S. P. Ong, G. Hautier, W. Chen, W. D. Richards, S. Dacek, S. Cholia, D. Gunter, D. Skinner, G. Ceder, K. A. Persson, *APL Mater.* **2013**, *1*, 011002.